Chapter 4

EXPERIMENTAL APPARATUS AND PROCEDURE

4.1 Superfluid Shock Tube Facility

The superfluid shock tube facility has been developed as a versatile tool for general researches in low-temperature thermo-fluid dynamic phenomena, in particular of superfluid helium. The shock tube was designed to be capable of operating with the $HeII$-filled test section immersed in superfluid helium in a cryostat. This device becomes the experimental facility that combine two extreme experimental situations, such as highly non-linear wave motion and cryogenic temperature. In the facility, a gasdynamic shock wave generated in saturated helium vapor impinges on a $HeII$ free surface, and consequently generates a transmitted compression shock wave and a thermal shock wave propagating through $HeII$.

From the technical point of view, the characteristic feature of the newly developed experimental facility is the capability of frost-contamination-free operations and repeated operations in a short time interval due to the application of the diaphragm-free quick-opening MO-valve system in the gasdynamic shock tube section. After completion of an experimental run the inside of the shock tube need not be exposed to atmosphere due to the elimination of the diaphragm replacement process. Accordingly, significant improvement can be expected by the application of an MO-valve driven diaphragm-free shock tube to researches of cryogenic fluids. The shock formation time in an MO-valve driven shock tube is inevitably longer than that in conventional diaphragm type shock tubes, $\sim 1ms$.

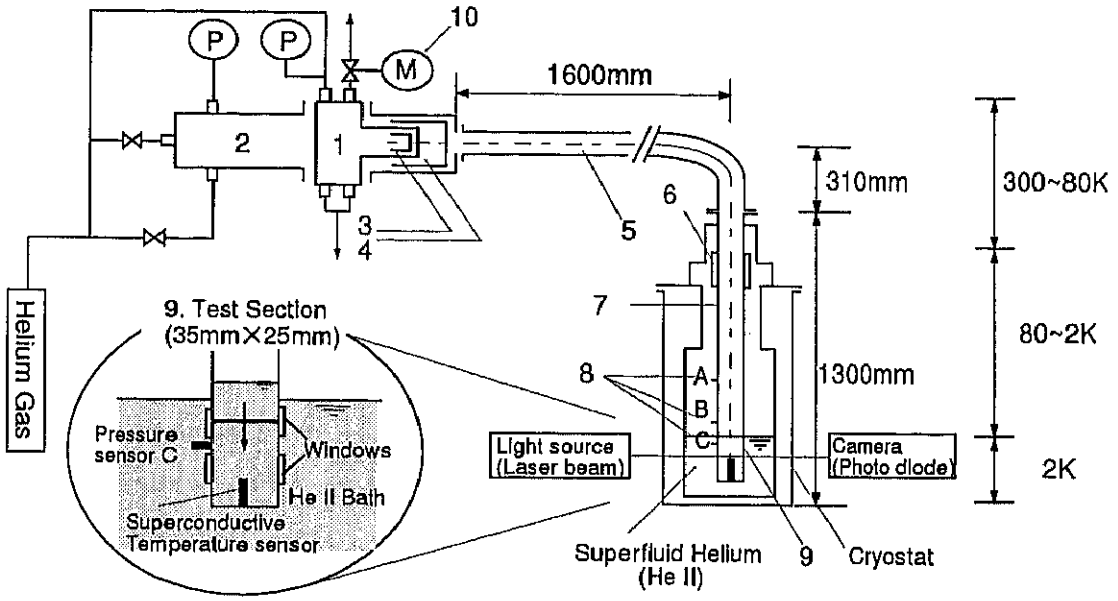

Figure 4.1: The schematic illustration of the superfluid shock tube facility. 1. MO-main valve, 2. High-pressure chamber, 3. Sub-piston, 4. Main-piston, 5. Low-pressure tube, 6. LN_2 tank, 7. Cryogenic shock tube, 8. Pressure transducers (A, B, C), 9. Test section filled with $HeII$, 10. Electro-magnetic pilot valve.

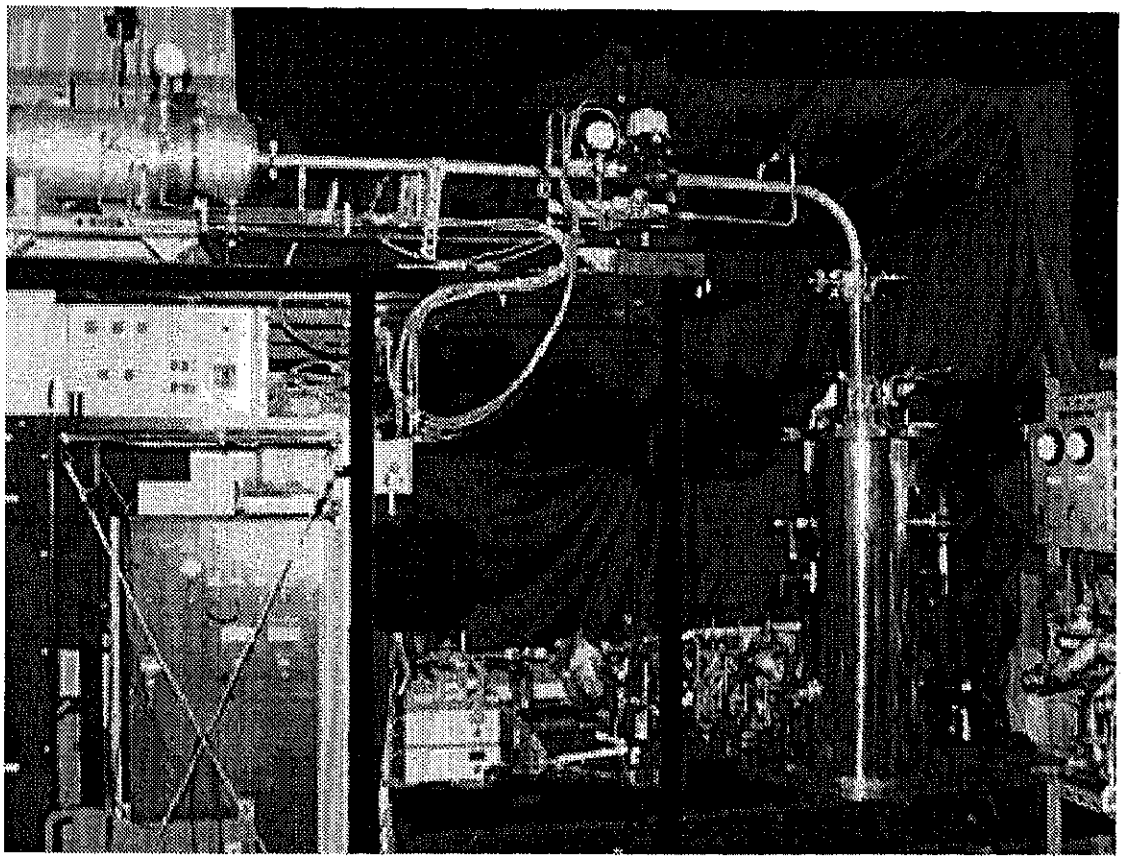

Figure 4.2: The photograph of the superfluid shock tube facility.

However, it causes no problem in operation because the pressure variation is measured just before the impingement as the initial condition of data analysis and the shock formation is quite reproducible in an MO-valve shock tube.

An overall view picture and a schematic illustration of the facility are shown in Figure 4.1 and Figure 4.2, respectively. The shock tube facility consists of two major parts, a diaphragm-free shock tube with an MO-valve and a $HeII$ cryostat with optical windows for visualization. A diaphragm-free shock tube is composed of two parts, a high-pressure chamber (driver section) charged with high-pressure gas and a low-pressure tube (driven section) charged with low-pressure gas.

4.1.1 High-pressure chamber

The structure of the high-pressure driver section is shown in Figure 4.3. It consists of two parts, the main-chamber with the main-piston, which plays the role of a diaphragm, and the sub-chamber with the sub-piston. The procedure to the valve opening to generate a shock wave is as follows:

(1) The high-pressure gas (driver gas) in sub-chamber is released into an open air by opening the electro-magnetic pilot valve to drive the sub-piston.

(2) The pressure behind the main-piston is instantly reduced as a result of fast movement of the sub-piston.

(3) The main-piston quickly moves backward to open because of the pressure difference between the both sides of it.

(4) The high-pressure gas in the main-chamber rapidly expands into the low-pressure tube and a shock wave is formed at the front.

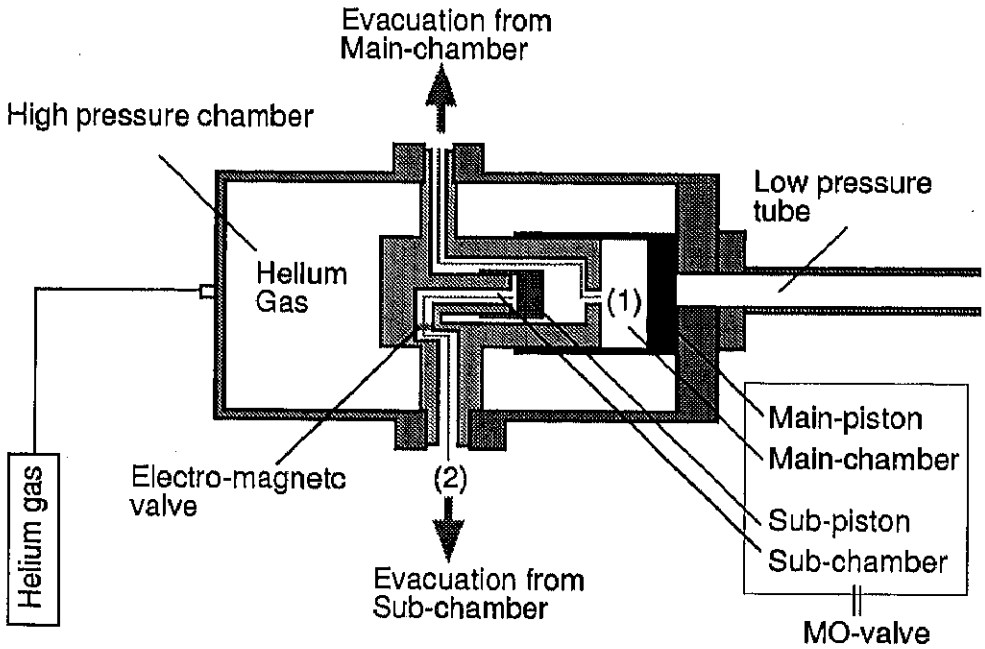

Figure 4.3: The structure of the high-pressure driver section.

The maximum design pressure of the high-pressure chamber is about 5.0 MPa. In the present study, driver gas is ^4He gas in most cases, and is sometimes N_2 gas.

4.1.2 Low-pressure tube (driven and test sections)

The schematic illustration of the low-pressure tube section is shown in Figure 4.4. The low-pressure tube consists of a horizontal straight tube section (1300 mm) with an inner diameter of 34.0 mm and a thickness of 2.0 mm, a bent tube section with a bent radius of curvature $R = 200$ mm, and a vertical tube section with a length of 1200 mm, all of which are made of stainless steel ($SUS304$). The horizontal and bent tube sections are exposed to room temperature atmosphere but the vertical tube is inserted in cryostat. The circular cross section of the bent tube section is converted to the rectangular one of the vertical tube part via the short adapter. It is, however, experimentally confirmed that there is no undesirable effect of the cross on the shock tube performance. The horizontal straight tube has a small outlet hole connected to a vacuum and a dump tanks.

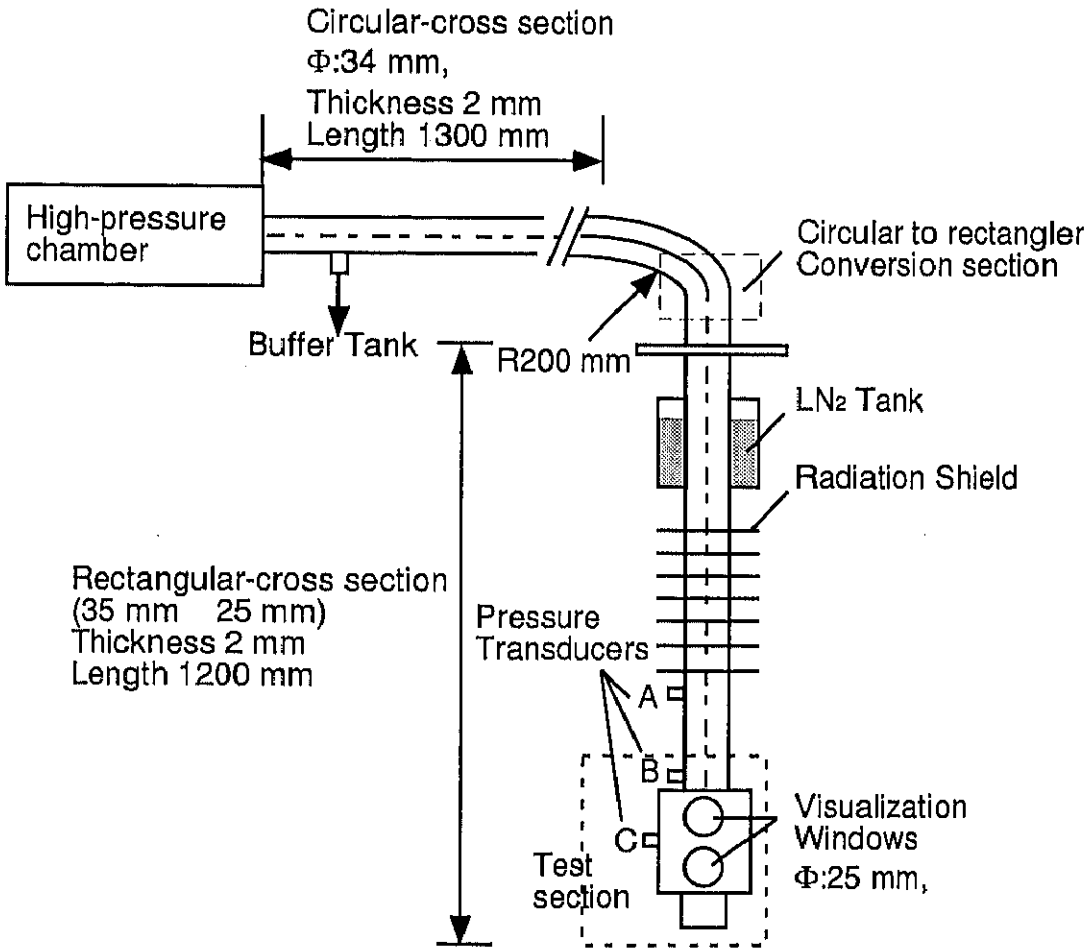

Figure 4.4: The schematic illustration of the low-pressure tube section.

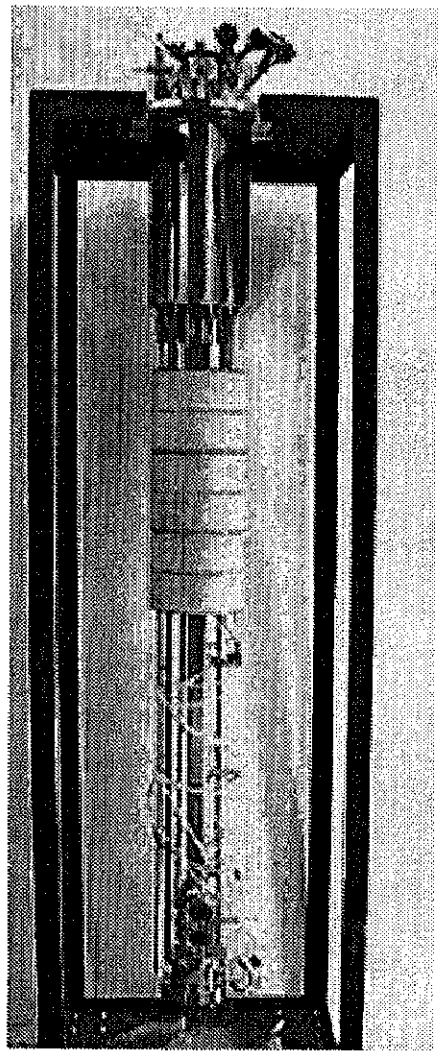

Figure 4.5: The photograph of cryogenic shock tube section.

The vertical section called the cryogenic shock tube with optical windows for visualization studies is inserted in the cryostat, which is shown in Figure 4.5, and is maintained at cryogenic temperature around 2 K at the bottom portion immersed in $HeII$ and at about 80 K at the top. A LN_2 tank is installed at the top to minimize the conduction heat leak from the room temperature portion of the cryostat to the 2 K portion of the shock tube.

The test section of the cryogenic shock tube is filled with $HeII$ and the rest of the low-pressure tube is charged with saturated helium vapor. The detailed structure of the test section is illustrated in Figure 4.6 and the photograph is shown in Figure 4.7. The cryogenic shock tube has a rectangular cross section (35 $mm \times 25$ mm) and is equipped with two pairs

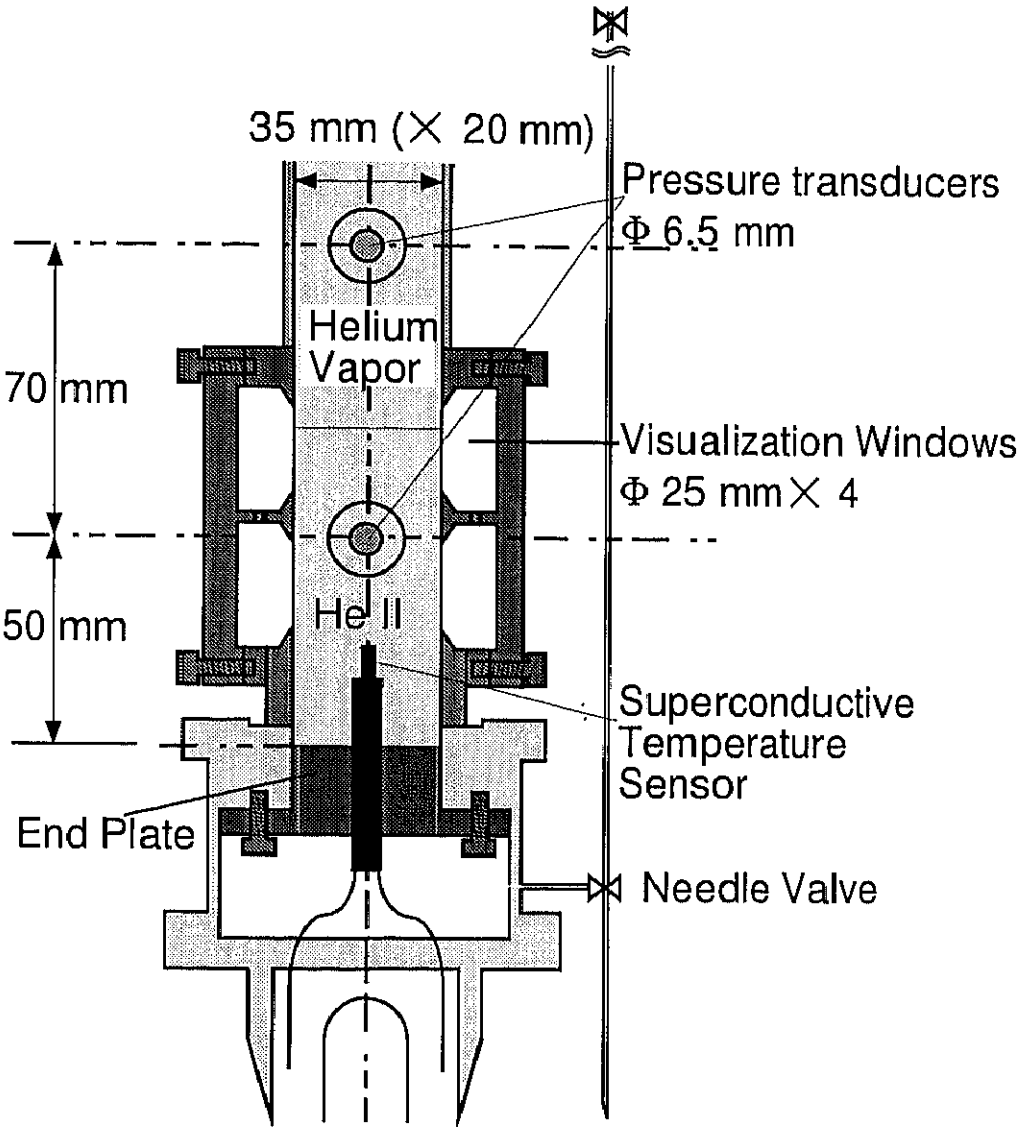

Figure 4.6: The detail structure of the test section.

of visualization windows with a diameter of 25 mm in the test section. Three piezo-electric pressure transducers are installed on the wall surface of the shock tube at 260 mm (transducer A), 120 mm (transducer B) and 50 mm (transducer C) from the bottom of the test section. A superconductive temperature sensor is supported on the end plate as shown in Figure 4.6.

Three piezo-electric pressure transducers measure the pressure variation and the shock propagating speed. The signal from the pressure transducer is also utilized as the signal of the trigger of visualization. The incident shock Mach number M_{SV} or the incident shock speed U_{SV} in the saturated helium vapor is measured by using upper two transducers of the three. For

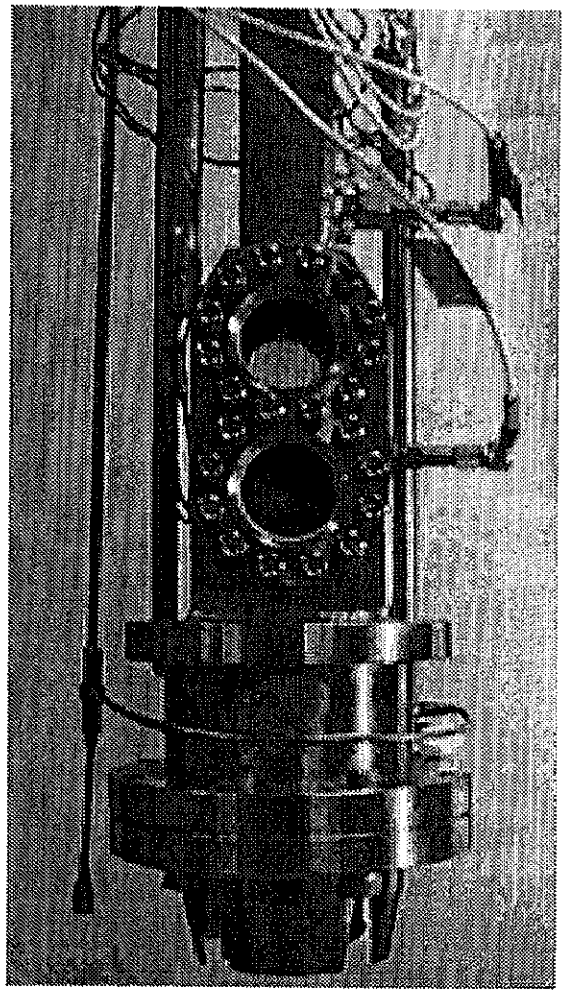

Figure 4.7: The photograph of the test section.

the measurement of the shock propagation speed (or shock Mach number) in $HeII$, we utilize the pressure signal detected by the pressure transducer and laser beam detector signals which are refracted by a shock front and detected by photo diodes. The temperature variation caused by both a transmitted compression shock wave (originating from a first sound mode) and a thermal shock wave (from a second sound mode) in $HeII$ are measured by the superconductive temperature sensor. The detail of the laser beam refraction method and the superconductive temperature sensor are described later (§ 4.2.2, 4.2.3).

4.1.3 Special feature of superfluid shock tube facility

The present superfluid shock tube has several advantages in the operation at cryogenic temperatures. The driven section of the shock tube can be maintained at the temperature down to 2 K due to the coexistence of saturated vapor with $HeII$. Accordingly, the viscosity of the gas is very small and thus the boundary layer effect can be minimized upon propagation. Furthermore, since helium vapor being a monatomic gas is very close to a perfect gas with a ratio of specific heats of 5/3, the physical states in the flow field can be accurately calculated by applying the simple theory of shock tube. If helium is used as a driver (subscript 4) and a driven (subscript 1) gases, the limiting shock Mach number is expressed in the following formula,

$$M_S = 4\,(T_4/T_1)^{\frac{1}{2}}$$

In the case that the driver gas temperature T_4 is at room temperature and the driven gas temperature T_1 is at cryogenic temperatures, a very large shock Mach number can be obtained. The superfluid shock tube can be applied in many areas of science and engineering, and even can be easily modified for wider range of applications. Shock waves with large Mach number and flows with large Reynolds number can be produced with this kind of experimental facility. Since the shock tube is filled with superfluid helium in the bottom portion in the present study, a gasdynamic shock can be made incident on a $HeII$ free surface and consequently some portion of it penetrates into $HeII$ and the rest reflects from it. The impedance matching for sound wave propagation through a gas-liquid interface of helium is much better than conventional gases, and thus a shock wave efficiently penetrates into $HeII$. Accordingly, the shock tube is also useful for the studies of a shock wave propagating under a strong density gradient state and of evaporation and condensation phenomena from/to $HeII$ free surface. Furthermore, such quantum mechanical phenomena as phase transitions across the λ-line ($HeII$-HeI) and across the $HeII$-solid helium boundary and a thermal shock wave caused by impinging a gasdynamic shock wave on the $HeII$ free surface can also be investigated.

4.1.4 Cryostat

The photo of the cryostat is shown in Figure 4.8 and its structural detail of the cryostat is illustrated in Figure 4.9. It is of a cylindrical shape with a height of 1310 mm and a diameter of 340 mm, and has three pair of windows for visualization as seen in the illustration. A pairs of optical windows of the innermost vessel and another pair of the outermost are respectively made superfluid tight and vacuum tight. The two window glass plates of the intermediate vessel cooled down to liquid nitrogen temperature are coated with IR absorbing thin film to absorb 300 K thermal radiation heat leak from the outside environment. The intermediate and innermost vessels have the tanks of liquid nitrogen for pre-cooling and as an auxiliary cryogen, respectively.

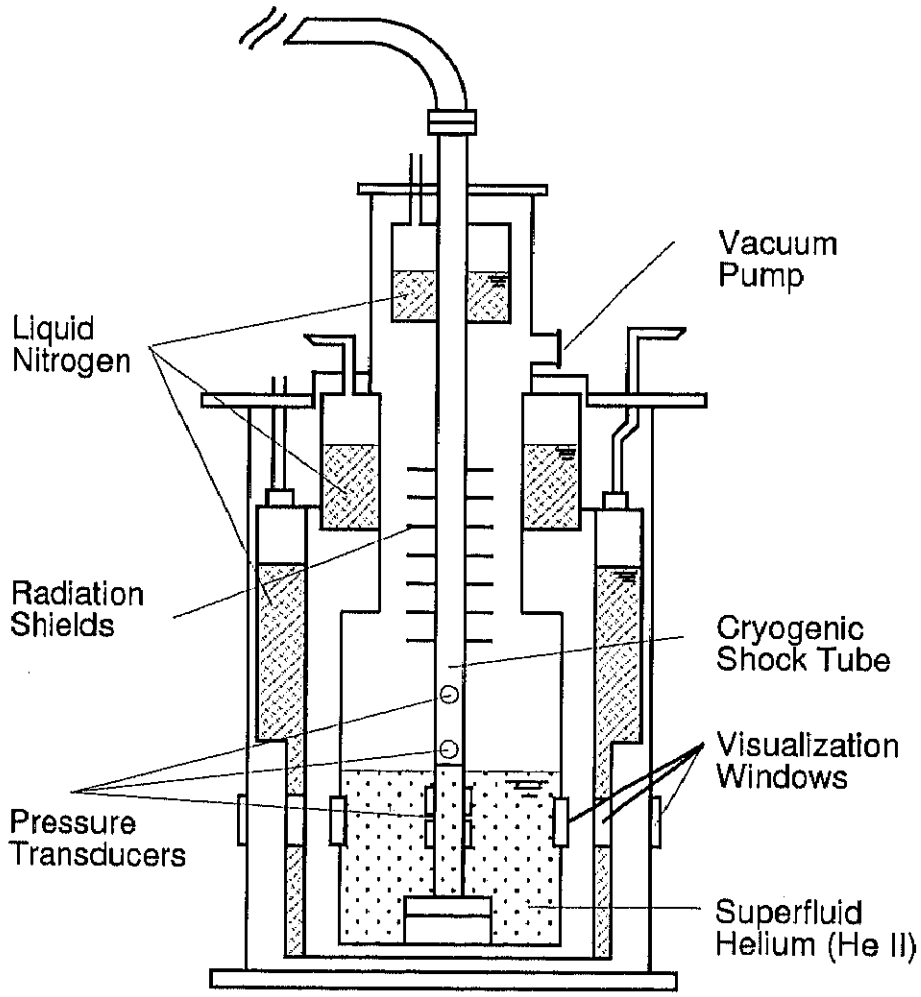

Figure 4.8: The cross-sectional view of cryostat section.

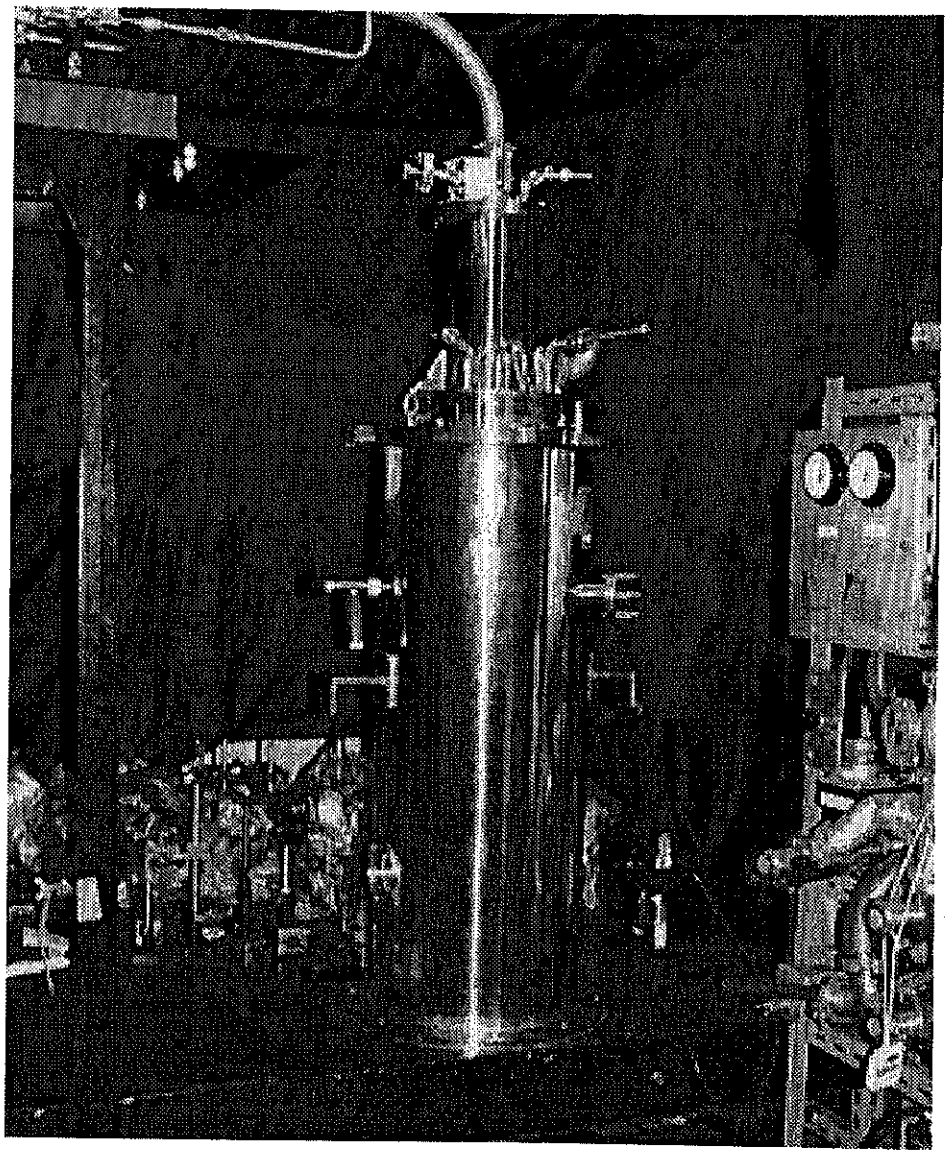

Figure 4.9: The photograph of the cryostats section.

The innermost vessel, which is the experimental space, is filled with liquid $HeII$. The cryogenic shock tube is immersed in $HeII$ in the innermost vessel. The inside of the cryostat must be evacuated down to 10^{-6} torr for vacuum-thermal-isolation. The vapor pressures of $HeII$ in the $HeII$ vessel and in the low-pressure tube of the shock tube are measured with capacitance-type high precision pressure transducers (MKS BARATRON TYPE 122A) in quiescent state. The cryostat must be set on a vibration-isolating table together with the optical visualization system. During each experimental run, the vapor pressure in the shock tube is kept constant with the pressure control valve system described in the next section.

4.1.5 Evacuation and automatic operation control system

The evacuation system consisting of three independent pumping units is attached to the facility as shown in Figure 4.10. The first one is connected to the $HeII$ bath where the cryogenic shock tube is located. As the temperature of $HeII$ is uniquely given as a function of saturated vapor pressure. Thus the temperature of $HeII$ in the $HeII$ bath is controlled with the pressure transducer (MKS BARATRON TYPE 122A) and the electric pressure control valve (MKS EXHAUST VALVE CONTROLLER TYPE 252C) connected to the evacuation line to the pump (VP-03) as shown in Figure 4.10. The second one evacuates the vapor in the low-pressure tube for the purpose of pressure control and of inducing a cold vapor flow from $HeII$ to cool down the room temperature part of the low-pressure tube of the shock tube. The third one evacuates gas from the buffer tank and the high-pressure chamber.

The operation of the facility is highly automated for saving manpower and safety. The operation from one shot to another is very simple, just pushing one switch. When the start switch is switched on to discharge a shock, the electromagnetic valves SV- 01 $\sim$ 05, AV-05 open and the valves AV- 02, 04 are shut to avoid abrupt pressure rise due to a shock wave. The sequence and the timing chart are shown in Figure 4.11.

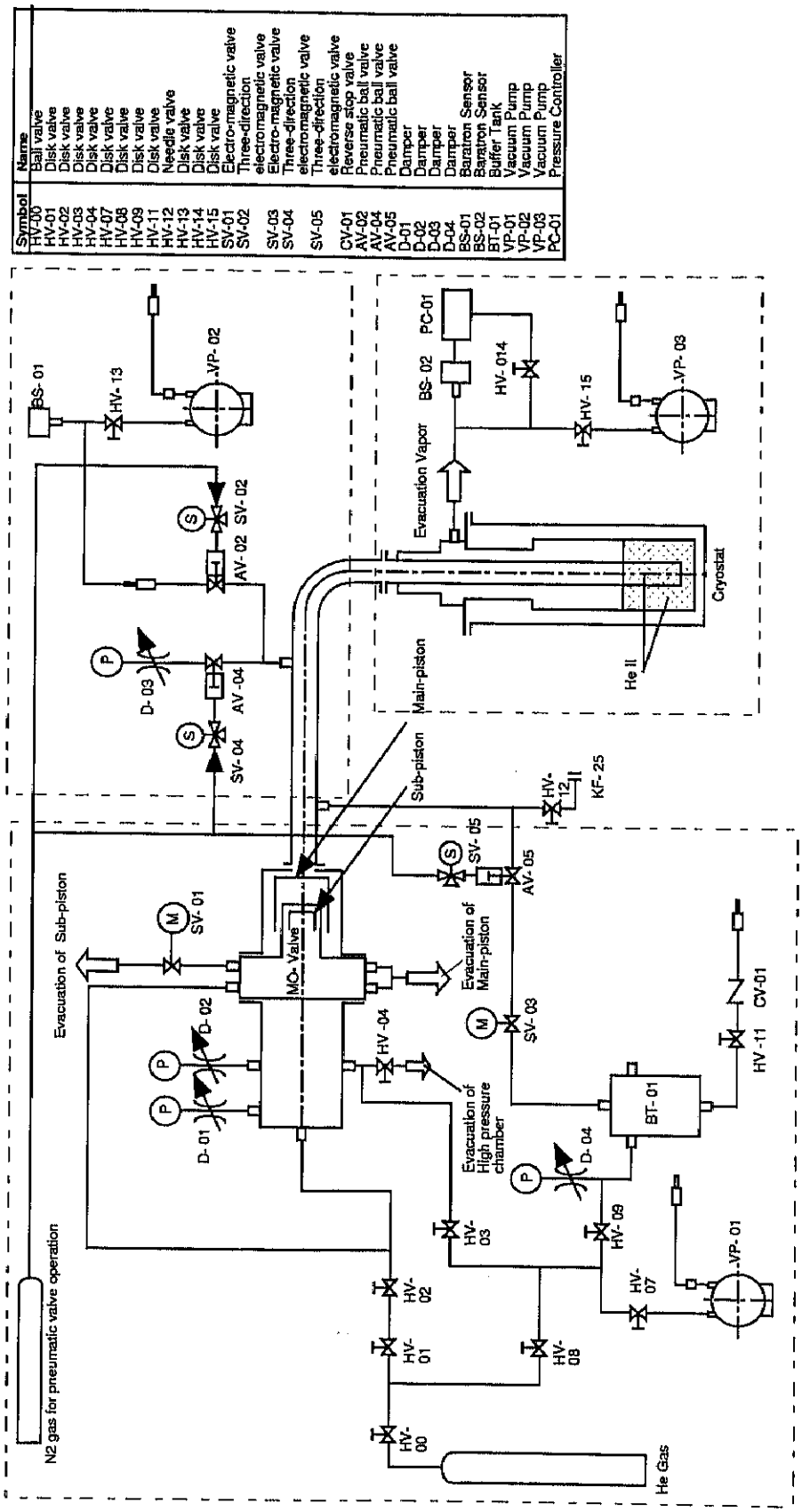

Figure 4.10: Evacuation and automatic operation system.

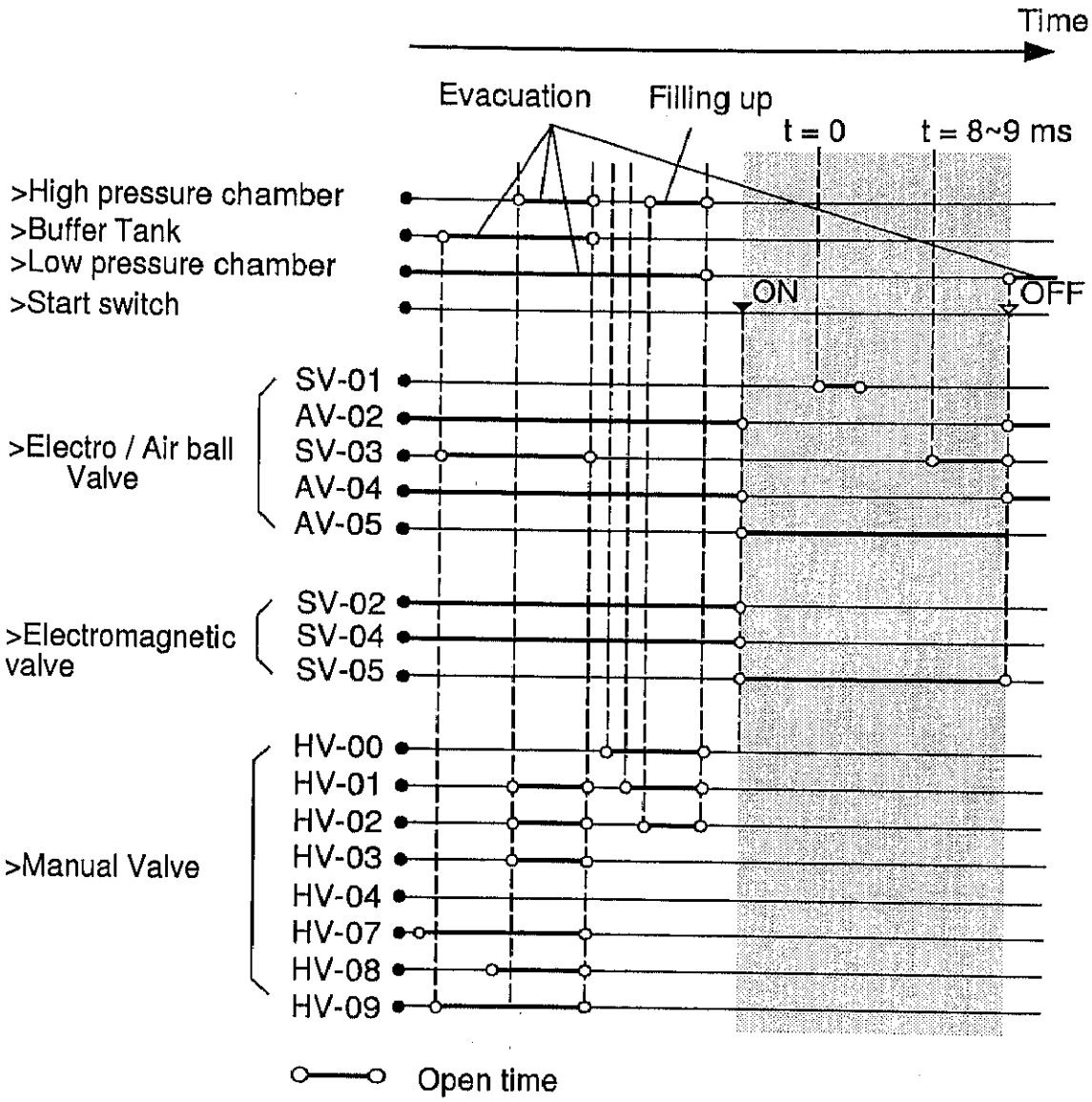

Figure 4.11: Schematic diagram of the sequence of automatic operation.

4.1.6 Outline of shock wave propagation in the shock tube

The impedance matching for shock wave propagation through a gas-liquid interface of helium is much better than those of conventional gases, and consequently a shock wave efficiently penetrates into $HeII$. Only a compression shock wave propagates into the liquid phase when the initial liquid phase is HeI. However, the two modes of shock waves propagate into the liquid phase when it is $HeII$. These two modes of shock waves can be cleaning distinguished by whether it is a compression or a thermal shock wave and by the propagation speed, 200 m/s for a compression shock and 20 m/s for a thermal shock. The schematic illustration of propagating shock waves in the cryogenic shock tube is shown in Figure 4.12. In this experiment, a gasdynamic shock wave (a-1) is generated in the helium vapor by using a diaphragm-free shock tube and then impinges on a free surface of $HeII$. Some portion of a shock wave (b-1) penetrates into $HeII$ as a transmitted compression shock wave and a remainder (a-2) is reflected back into the vapor. And at the same time, a thermal shock wave (c) is also generated and propagates through $HeII$ at slower propagation speed than a compression shock. Accordingly, thermal shock wave propagates through liquid helium compressed by a transmitted compression shock wave. A reflected compression shock wave (b-2) from the bottom of the shock tube again impinges on a free surface. Major part is re-reflected from a free surface and re-propagates into a $HeII$ downward as a rarefaction wave (b-3) and some portion of a reflected shock wave penetrates into the helium vapor phase as a transmitted gasdynamic shock wave (a-3).

If a strong compression shock wave propagates through $HeII$, a thermal shock wave cannot be generated. In this case, $HeII$- HeI λ-phase transition takes place, and accordingly, a thermal shock wave is not excited.

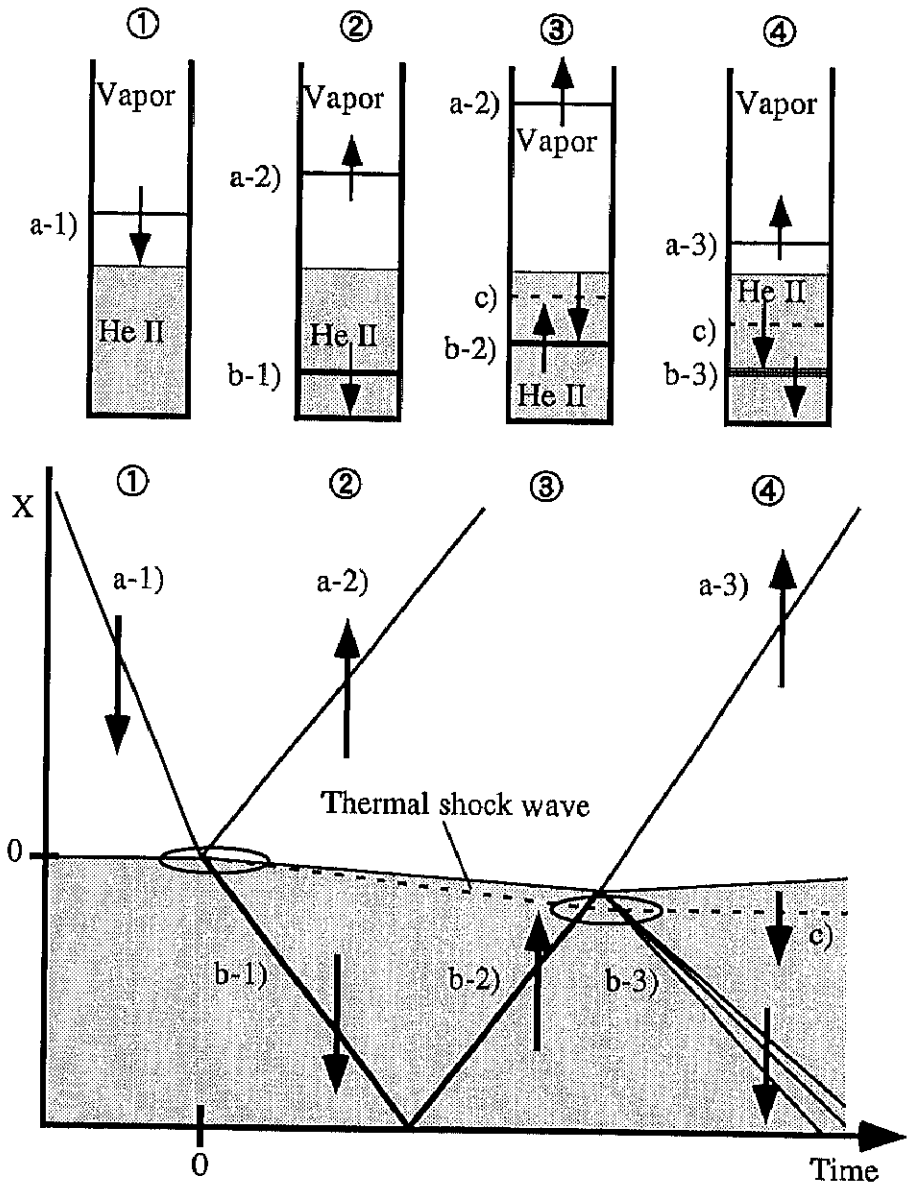

Figure 4.12: The schematic illustration of propagating shock waves in the cryogenic shock tube.

4.2 Instrumentation

4.2.1 Piezo-electric pressure transducer

The transducer consists of a quartz pressure element coupled to a special $MOSFET$ amplifier circuit to allow operation at cryogenic temperatures. The photo of the pressure transducer is shown in Figures 4.13 and 4.14. Its specification are as follows at 20 K,

Table 3: The specification of piezo-electric pressure transducer

RANGE	psi kPa	0.02~100 0.14~690	0.2~1000 1.4~6900	1~5000 6.9~34500	2~10000 14~69000
MODEL NO.		M102A10	M102A11	M102A14	M102A13
SENSITIVITY	mV/psi mV/kPa	50 7.2	5 0.72	1 0.145	0.5 0.072
RESOLUTION	psi kPa	0.002 0.014	0.02 0.14	0.1 0.69	0.2 1.4
MAXIMUM DYNAMIC PRESSURE	psi kPa	2000 13800	15000 103500		
LINEARITY RESONANT	%	<1	<1		<2
FREQUENCY RISE TIME	kHz μsec	>250 <2	>250 <2		
DISCHARGE TIME RESPONSE	sec	>1	>2		>5
LOW FREQUENCY RESPONSE	Hz	0.5	0.3		0.1
TEMPERATURE COEFFICIENT		-423 to 212 ° F(-253 to 100° C) / <0.06%° F(<0.018%° C)			
OUTPUT IMPEDANCE		<500 ohm / 3 to 8			
Inch.(3/8-24)		102A10	102A11	102A14	102A13

Note that the transducer can not be calibrated at 2.0 K of $HeII$ temperature. It seems, however, that the effect of cryogenic temperature on the performance is very small. Accordingly, the calibrated performance at 20 K is adopted in the present experiment because no simple calibration method has been found so far.

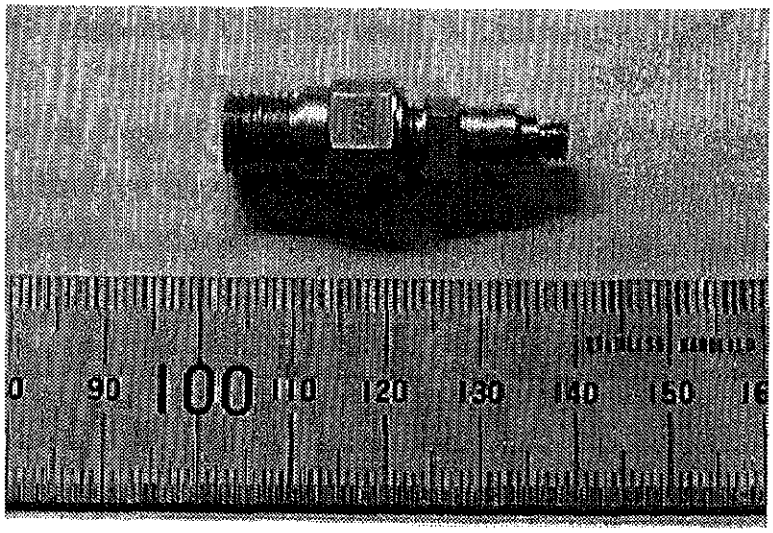

Figure 4.13: The photograph of the piezo-electric pressure transducer1.

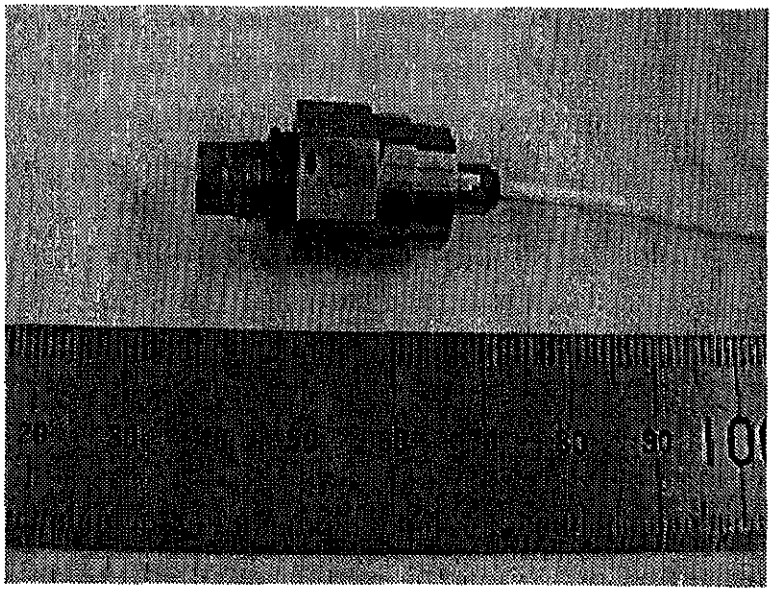

Figure 4.14: The photograph of the piezo-electric pressure transducer2.

4.2.2 Superconductive temperature sensor

A superconductive temperature sensor which has high temperature sensitivity and short response time is used to measure highly transient heat transport in *HeII*. This sensor measures the temperature variation by utilizing the abrupt change of the resistivity of thin superconductive metal film due to superconductive transition. Superconductive phenomenon, occurs in a number of metals and oxides when all the temperature, the magnetic field and current density are below certain critical values. The electrical resistivity of the material vanishes and the Meissner effect appear in the superconductive state. If one of these three quantities exceeds a critical value, superconductive transition from superconductive state to normal state occurs.

Superconductors can be classified into two types, *TypeI* superconductor and *TypeII* superconductor. *TypeI* superconductor is pure metals and *TypeII* superconductor is alloys or oxides. The former exhibits an almost discontinuous change from normal state to superconductive state, and vice versa. The latter exhibits gradual superconductive transition. Figure 4.15 illustrate the ideal resistivity variation of *TypeI* superconductor.

If one of the quantities exceeds a threshold value, the superconductive state breaks down and then electric resistance suddenly increases up to the normal resistance as the increase of the quantity. It is well known that pure tin is a *TypeI* superconductor, of which superconductive transition occurs near 3.7 K within the temperature range of no more than 10^{-3} K.

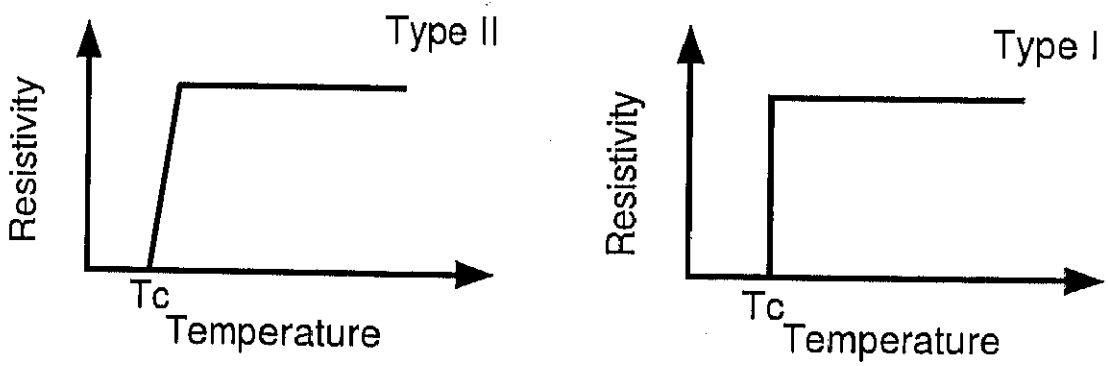

Figure 4.15: Schematic illustration of the resistivity variations with temperature of *TypeI* and *TypeII* superconductor. T_{cr} is the critical temperature.

It exhibits quite a sensitive resistivity change to the temperature variation within the temperature range. Tin is utilized for a sensitive bolometer for the detection of infrared radiation.

The temperature sensor for the temperature measurement of highly transient thermo-fluid dynamic phenomena, such as a compression and a thermal shock waves in $HeII$, would require the superconductive transition to occur within several hundreds mK at arbitrary temperatures below $T_\lambda = 2.17\ K$. Superconductive transition of $TypeII$ superconductor seems adequate for the temperature measurement in $HeII$. In the present study, thin metal film consisting of gold and tin is used. Gold which does not become a superconductor acts as impurity for tin and depresses the superconductive transition of the film. The transition can be made more gradual at below T_λ.

Figure 4.16 shows a schematic drawing of a superconductive temperature sensor used in the present study. Figure 4.17 shows the photograph of temperature sensor. It resembles a conventional hot wire probe in shape to be used for the flow velocity measurement in aerodynamic experiments. The temperature variation is measured with the sensing element, on which surface a superconductive thin film is formed. It consists of gold and tin film with a thickness of 1000 $\AA$ for Tin and 230 $\AA$ for gold formed by vacuum deposition on a side surface of quartz fiber with a length of 2.0 mm and 40 μ m in diameter. The quartz fiber is glued with silver paste to the metal needles. Since the heat capacity of the sensing element is quit small, the response time of the sensor is very short (not more than 10 μ s). A particular feature of this sensor is its very high sensitivity and rapid time response within a few μ sec. Accordingly, the temperature variations induced by a compression and a thermal shock waves can be measured with the sensor. However, this technique requires low-temperature environment, especially $HeII$ environment. So, it cannot be used in vapor phase at high temperatures.

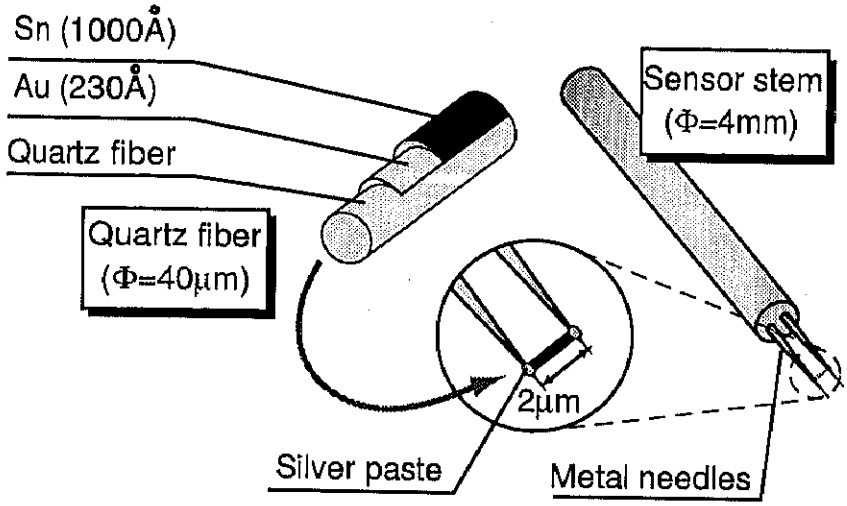

Figure 4.16: Schematic illustration of superconductive temperature sensor.

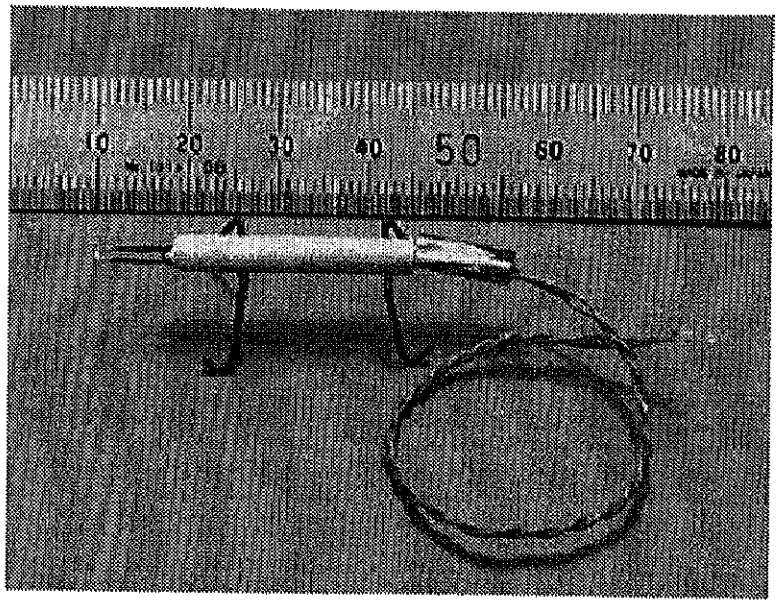

Figure 4.17: The photograph of superconductive temperature sensor.

4.2.3 Semiconductor laser and photo diode

To detect the time variation of the density, a method of laser beam transmission through the test field is used. When the density of the fluid changes, the refractive index also changes, which causes some deflection of laser beam. Laser beam is introduced into the test section of the shock tube through the optical windows, and the intensity is detected by a PIN photo diode at the opposite side outside of the cryostat. Such variations in the physical properties as the density of the fluid cause the deflection and scattering of the laser beam, which results in drop in the output signal from the photo detector.

4.3 Visualization

4.3.1 Principle of Schlieren visualization method

The basic idea of the Schlieren method is that some potion of light refracted in an observation field is interrupted on its way to a screen and therefore the part of the field through which this light passes is locally seen dark. The principle of the Schlieren method is illustrated in Figure 4.18. The light from a light source with a size of $a \times b$ is made a parallel light bundle by means of the lens L_1 (focal length f_1) and then passes through the observation field. It is converged by the lens L_2 (focal length f_2) and forms the light source image with a size of $a' \times b'$ on its focal plane, where a knife edge interrupts a part of the light. The image of an object in the observation field is finally formed on a screen by lens L_3. If there is no variation in the index of refraction in the observation field, the light passes through any point in the field is uniformly interrupted by the knife edge and comes to a middle brightness on the screen. Now, lets consider the case that the light which passes through a point P in the observation field is refracted downward by inhomogeneity in the refractive index or in the density as illustrated by the broken lines in Figure 4.18. Then the light is interrupted still more by the knife edge and consequently the point Q which is the image of the point P comes to be dark. In the contrary case when the light is refracted upward the point Q comes to be bright. Thus the light refracted vertically with respect to the knife edge gives some change in the light intensity on the

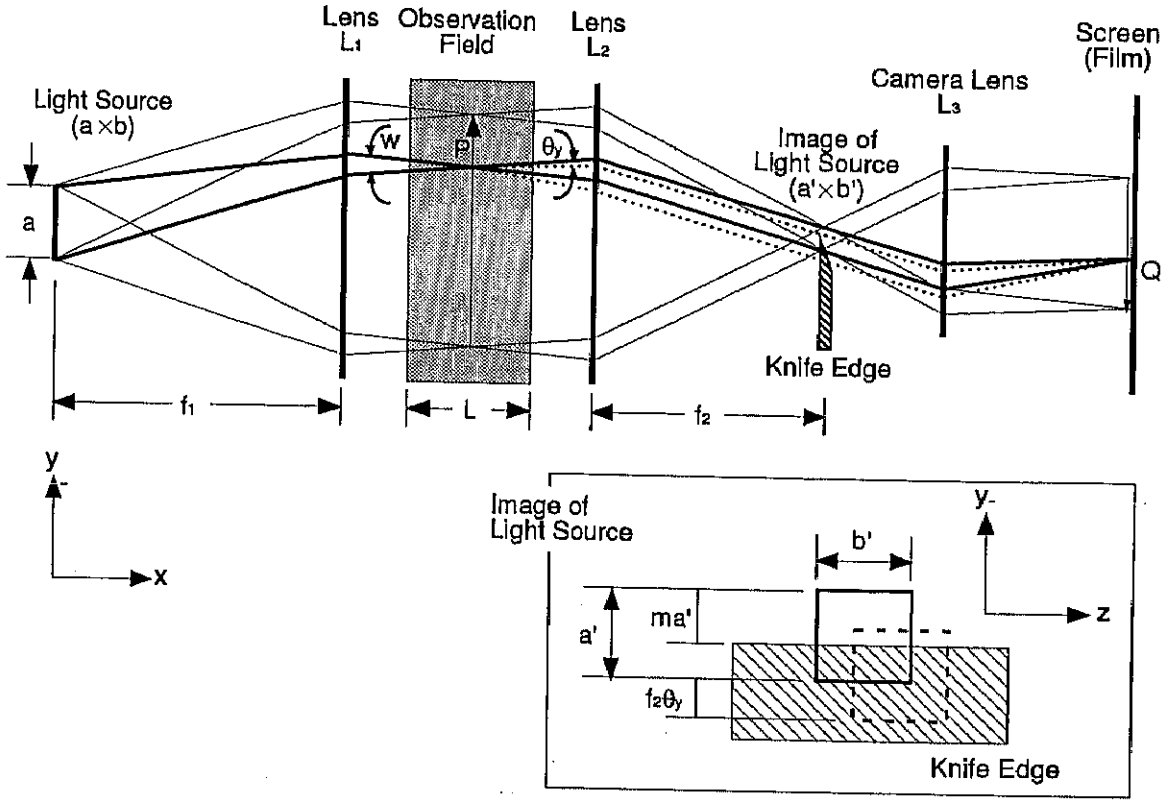

Figure 4.18: Schematic illustration of the principle of Schlieren visualization method.

screen. Schlieren image with enhanced light and shade is constructed in this manner.

If the light source image is originally interrupted by its width a'-ma' (m: uninterrupted portion) by the knife edge in a quiescent state and then shifted by its position $f_2\theta_y$ as a result of the refraction in the observation field (see the inset of Figure 4.18), the intensity change on the screen is given by ,

$$\frac{\Delta E}{E} = \frac{f_2\theta_y}{ma'} = \frac{f_2}{ma'}\int_0^L \frac{\partial n}{\partial y}dx = \frac{f_2 K}{ma'}\int_0^L \frac{\partial \rho}{\partial y}dx \qquad (4.1)$$

where θy is the total angle of deflection, n is the index of refraction, ρ is the density, L is the depth of the observation field and K_G is the Gladstone-Dale constant of the medium in the observation field. It is thus seen that the light intensity appeared in a photographic picture is in proportion to the first spatial derivative of the density in the field. The sensitivity s of the image on the screen is given by,

$$s = \frac{d\left(\Delta E/E\right)}{d\theta_y} = \frac{f_2}{ma'} \tag{4.2}$$

The width of image of light source a' is

$$a' = wf_2 = \frac{af_2}{f_1} \tag{4.3}$$

and therefore the sensitivity is given by,

$$s = \frac{f_1}{ma} \tag{4.4}$$

Thus the sensitivity is found to be directly proportional to the focal length of a concave mirror to make a parallel beam, be inversely proportional to the size of a pin hole at the light source and the ratio of uninterrupted portion by the knife edge, m.

4.3.2 Shadowgraph method

Shadowgraph method is another visualization method that the shadow of a beam due to a density change in the observation field is directly projected on a screen. In a Shadowgraph optics, a point-shaped light source may be used instead of a parallel light beam, and a knife edge is removed. The optical system and procedure are rather simple in this technique. The darkness in a Shadowgraph is in proportion to the second derivative of the density distribution, and the sensitivity is of medium grade, being less sensitive than the Schlieren method. Consequently, for the visualization of a $HeII$-vapor interface region, the Shadowgraph method is usually more relevant than the Schlieren method because the variation in the density is too large in the interface region. However, the Schlieren method is employed for visualizing the variation in the density in bulk $HeII$ caused as a result of noisy boiling.

Schlieren and Shadowgraph methods are used to visualize the variation of the density, equivalently the index of refraction in the observation field by converting the variation in the index of refraction to the light intensity variation on the screen, as seen from the above description. Thus they are not necessarily adequate to quantitative measurements, though they are

generally applied to the observation of a flow field. They are of great use for gaining global information in the whole observation field.

4.3.3 Optical arrangement

The arrangement of the Schlieren optics is shown in Figure 4.19. A combined light source with a pinhole is composed of a super-high pressure mercury lamp and a magnesium-spark light source. The continuous light source of mercury lamp by arc discharge is used for the system alignment and video recording. The magnesium-spark light source with a spark duration of 3 μs is utilized for the high speed still photographing. The two concave mirrors, the Schlieren heads, which are made of *Pyrex* coated with vacuum deposited aluminum with protective membrane of silicone are used to make a parallel beam. They have an effective aperture diameter of 150 mm and a focal length of 1510 mm. The knife edge, which is ratable around a horizontal axis to easily adjust the direction of the maximum density gradient in the observation field, cuts off a part of light to produce a Schlieren image. A 35 mm still camera mounted at the end of a long bellows is integrated with the knife edge on a common stand. In the case of Shadowgraph visualization, a knife edge is removed.

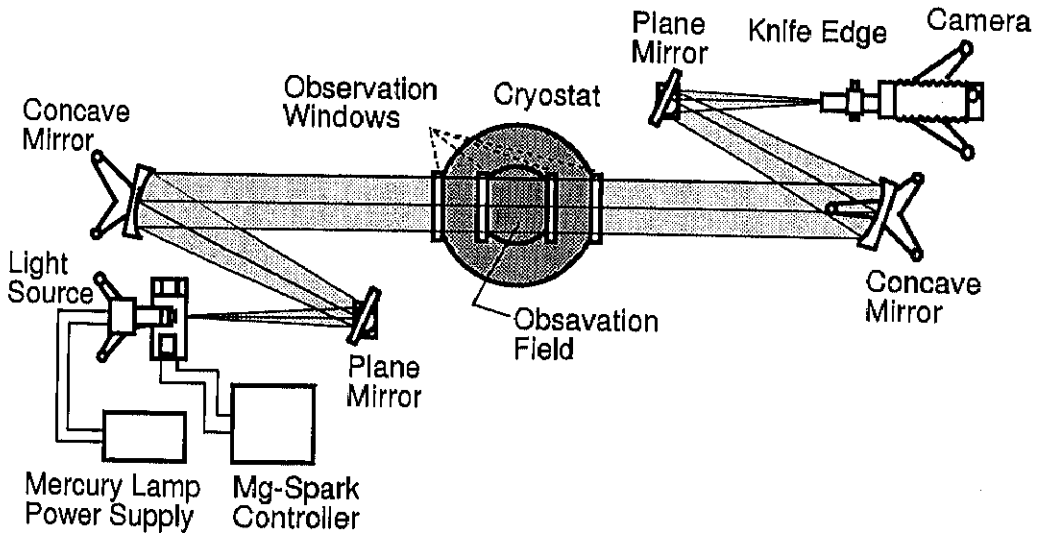

Figure 4.19: The arrangement of Schlieren optics. In the Shadowgraph visualization, a knife edge is removed.